NRC Research Press

ARTICLE

Effect of transverse flow in porous medium on heat exchanger simulation optimization

Yang Liu, Chao Yu, Sicheng Qin, Xiangjie Wang, and Jiarun Lou

Abstract: To improve the accuracy of heat exchanger computational fluid dynamics (CFD) simulations, the transverse resistance coefficient of the cold side and the hot side of the water-cooled charge air cooler (WCCAC) is calculated using the fin element method, and the influence of several common factors on the resistance coefficient of the fin element is analyzed. The transverse resistance coefficient obtained from the simulation of the fin element is substituted into the WCCAC model and compared with experimental data. It was found that the fin element method can simulate the flow field of the WCCAC accurately, and the simulation results were closer to the experimental curve compared with the empirical method. This study provides guidance for the optimal design of the heat exchanger and is helpful to shorten the development time and to save costs.

Key words: heat exchanger, water cooled charge air cooler, porous medium, fin element, computational fluid dynamics.

Résumé : Pour augmenter la précision de la simulation MFN des échangeurs de chaleur, la méthode des éléments à ailettes permet de calculer le coefficient de résistance transversal du côté froid et du côté chaud du refroidisseur d'air de suralimentation à eau, et d'analyser l'influence de plusieurs facteurs communs sur le coefficient de résistance de l'élément à ailettes. La résistance transversale calculée à partir de la simulation de l'élément à ailettes est remplacée par le modèle WCCAC et comparée aux données expérimentales. Il s'avère que la méthode de l'élément à ailettes est en mesure de simplifier le champ d'écoulement de la WCCAC de manière précise, et que les résultats de la simulation se rapprochent de la courbe expérimentale par rapport à la méthode empirique. Elle apporte des indications en vue d'une conception optimale de l'échangeur de chaleur et sert à réduire le temps de développement et à réaliser des économies. [Traduit par la Rédaction]

Mots-clés : échangeur de chaleur, refroidisseur d'air de suralimentation refroidi par eau, milieu poreux, élément à ailettes, mécanique des fluides numérique.

1. Introduction

In a typical heat exchanger, the intercooler is used to cool the high temperature and high pressure air from the supercharger, which can greatly reduce pollutant emissions and improve the dynamic performance of the diesel engine (Mezher et al. 2013). At present, most researchers use the software Fluent and other multidimensional simulation software to design and calculate heat transfer and pressure loss of heat exchangers (Kumar et al. 2012; Balaji et al. 2015). Kumar et al. (2012) used ANSYS software to analyze the heat dissipation performance of fins of a fin tube intercooler. When aluminum was used, the surface heat transfer coefficient was 19.73% higher than that of copper. When changed from copper to bronze, the surface heat transfer coefficient decreased by 0.53%. Dong et al. (2012) analyzed the flow field and pressure drop of a gas turbine intercooler with the help of computational fluid dynamics (CFD) technology. Uysal et al. (2012) conducted a numerical study on the momentum and thermal characteristics of the connecting hose of a fiat engine intercooler. Cuevas et al. (2011) carried out relevant experimental tests on cars equipped with low-pressure exhaust recirculation to determine the impact of triangular straight fins and shutter fins on the thermal and hydraulic performance of intercoolers. Hribernik and Moskwa (2000)

Y. Liu and C. Yu. Changchun Institute of Optics, Fine Mechanics and Physics, Chinese Academy of Sciences, Changchun 130033, China.

S. Qin, X. Wang, and J. Lou. School of Mechanical and Aerospace Engineering, Jilin University, Changchun 130022, China.

Corresponding author: Chao Yu (email: yuchao17@mails.jlu.edu.cn).

established the NTU efficacy method and the 2D model method to calculate and analyze the properties of air cold-plate-fin cross-flow heat exchangers, and compared the advantages and disadvantages of the two methods.

However, it is difficult to simulate the whole structure of the heat exchanger because of the complex structure and large number of fins. Also, large data sets make the ordinary microcomputer computation efficiency low or the simulation cannot run at all. To reduce the simulation requirements and realize the rapid and effective flow field analysis of heat exchangers, most of the current simulation calculations need the help of a porous media model. The simulation method adopted by most researchers is to downplay the influence of flows in the second and third directions and focus on the main flow direction of incoming flows in porous media (Dong et al. 2007*a*). Guo et al. (2008) directly set the viscosity and inertia resistance coefficients in the second and third directions at two or three orders of magnitude in the main flow direction to simulate the resistance of fluid media in order to roughly estimate the resistance coefficients. While mainly considering the influencing factors of the main flow direction. However, according to this semi-empirical method, the magnitude of the resistance coefficient has a large span and does not indicate which simplified magnitude of fluid medium should be adopted. Therefore, many uncertain effects will be produced in the actual heat exchanger simulation calculation. Usually the fin height of the heat exchanger is <1% of the flow direction length, and ignoring the fluid medium in the direction of the fin height of the third tap will not cause a great influence to the whole simulation (Dong et al. 2013). But compared with the third direction heat exchanger, there is usually a larger transverse size, and the accuracy of the simulation of the transverse shunt in the flow passage will directly affect the simulation accuracy of the heat exchanger.
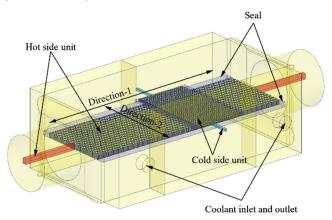
The water-cooled intercooler contains both gas and liquid fluid media, and its structure and principle are relatively complex (Kays and London 1984). Therefore, in this study, the water-cooled intercooler was choosen as the carrier for simulation research. The viscous and inertial drag coefficients of rectangular cross-toothed fins were analyzed by building main flow direction and transverse flow direction models of the hot and cold sides of a water-cooled intercooler. The resistance coefficients obtained by the solution method and the two groups of empirical resistance coefficients were put into the overall model of the water-cooled intercooler for Fluent simulation to calculate its pressure parameters. Finally, the calculated results were compared with the test data of the intercooler, and the influence of transverse flow on heat exchanger design was studied.

2. Establishment of simulation model

2.1. Porous media model

A momentum source term was added to the momentum equation to simulate the action of the porous

Fig. 1. Structure of the water-cooled charge air cooler. [Colour online.]

media. Where S_i is the source term of the momentum equation; v_j is the velocity vector; D_{ij} and C_{ij} are the matrix elements of the viscous resistance coefficient and inertial resistance coefficient, respectively. For simple homogeneous porous media, the momentum source term can be simplified into eq. 2 (Dong et al. 2007*b*). Where $\frac{1}{\alpha}$ is the coefficient of viscous resistance and C_2 is the coefficient of inertia resistance.

$$(1) \qquad S_i = -\left(\sum_{j=1}^{3} D_{ij}\mu v_j + \sum_{j=1}^{3} C_{ij}\rho v_{\mathrm{mag}} v_j \right)$$

$$(2) \qquad S_i = -\left(\frac{\mu}{\alpha} v_i + C_2 \frac{1}{2} \rho v_{\mathrm{mag}} v_i \right)$$
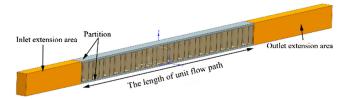
According to the semi-empirical simplified solution method provided by some researchers and the software Fluent, the coefficient of viscous resistance and inertial resistance in the second direction (Direction-2 in Fig. 1, hereinafter referred to as D2) and third direction (Direction-3 in Fig. 3, hereinafter referred to as D3) can be amplified by 100 or 1000 times of that in the first direction for calculation.

2.2. Element model and boundary conditions

In a water-cooled intercooler, a typical plate-fin heat exchanger is composed of the air chamber, water chamber, hot side cooling zone, cold side cooling plate, and seal. The hot side has 10 layers of scattered tropics, while the cold side has nine layers of hot plates. The air in the hot side flows horizontally, while the coolant flows in a secondary U-shape in the cold side. Theoretically, when solving the parameters of the porous medium of the heat exchanger, it is necessary to simulate all the flow paths on the hot and cold sides of the heat exchanger, which requires an extremely large number of calculations, but the current development level of computer hardware makes it difficult to accomplish such a task. In this paper, the fin element method used to solve the drag coefficient

Fig. 2. Transverse flow fin element of the hot side. [Colour online.]

Fig. 3. Geometric parameters of the fin. [Colour online.]
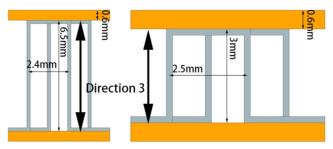

simplifies the solution of a heat sink layer to a fin unit by setting the period and symmetrical boundary.

Taking the hot side of the intercooler as an example, the length of the main flow direction element is equal to 300 mm of fin length. To study the influence of a transverse shunt on the calculation, it is necessary to establish the transverse flow element of the hot side (Fig. 2), whose passage length is 94 mm of the fin width. The bulkhead is 0.6 mm thick, the fin thickness is 0.2 mm, the flow direction pitch on the hot side is 2 mm, and the cold side is 3 mm. The length of the inlet and outlet extension zone is five and seven times of the hydraulic diameter of the fin. The geometric parameters of the fins on the hot side and cold side are shown in Fig. 3.

As the overall model size of the intercooler is large and its requirements for mesh quality are not high, the maximum mesh size in GAMBIT was generally <0.8 in order to meet the simulation requirements. The precision of the viscous resistance coefficient and inertial resistance coefficient will determine the accuracy of the porous media model, which is greatly affected by the mesh quality of the finned element model, so the mesh quality of the element model should be improved as much as possible (Chen et al. 2013). The hot side unit body model meshed by GAMBIT was established at 1/5

of the flow path length of the hot side main flow direction (Direction-1 in Fig. 1, hereinafter referred to as D1). Five boundary layers with a starting thickness of 0.01 mm and an increment of 1.01 were established on the surface of the fin (Fig. 4). The unit body model was divided into grids with grid meshing size of 0.1. Finally, the number of final grids in the hot side D1 direction unit was 3 147 600. The grid density was 807 cells/mm^3. Since the structure of each part of the three kinds of unit bodies on the hot side D2 and the cold side D1 and D2 is similar to that of the hot side main flow unit, only the number of grids is different, so it will not be described. The physical property parameter settings are as follows: The hot pressurized air side was 120 °C; the dynamic viscosity was 22.84×10^{-6} kg/m·s; the density was 2.656 kg/m^3; the coefficient of thermal conductivity was 0.0325 w/m·k. The cold side was glycol cooling fluid; the dynamic viscosity was 7.14×10^{-4} kg/m·s; the density was 1013 kg/m^3; coefficient of thermal conductivity was 0.4043 w/m·k (Song et al. 2014; Yu et al. 2018). In this research, the k–ε turbulence model was used for simulation by Fluent, and the transport equation of the standard k–ε model is as follows (Yu et al. 2018):

$$(3) \quad \begin{cases} \dfrac{\partial(\rho k)}{\partial t} + \dfrac{\partial(\rho k u_i)}{\partial x_i} = \dfrac{\partial}{\partial x_j}\left[\left(\mu + \dfrac{\mu_t}{\sigma_k}\right)\dfrac{\partial k}{\partial x_j}\right] + G_k + G_b - \rho\varepsilon + S_k \\[2ex] \dfrac{\partial(\rho\varepsilon)}{\partial t} + \dfrac{\partial(\rho k u_i)}{\partial x_i} = \dfrac{\partial}{\partial x_j}\left[\left(\mu + \dfrac{\mu_t}{\sigma_\varepsilon}\right)\dfrac{\partial\varepsilon}{\partial x_j}\right] + C_{1\varepsilon}\dfrac{\varepsilon}{k}(G_k + C_{3\varepsilon}G_b) - C_{2\varepsilon}\rho\dfrac{\varepsilon^2}{k} + S_\varepsilon \end{cases}$$

The following values were used for the standard k–ε model:

$$C_{1\varepsilon} = 1.44 \quad C_{2\varepsilon} = 1.92 \quad C_{3\varepsilon} = 0.09 \quad \sigma_k = 1.0 \quad \sigma_\varepsilon = 1.3$$

3. Analysis of drag coefficient of fin element

3.1. Influence of flow length on drag coefficient

Taking the hot side D1 direction unit as an example, the influence of the period boundary and symmetrical boundary on the calculation was studied. The actual flow length in the D1 direction of the hot side dispersing zone of the intercooler was 300 mm. To verify whether reducing the runner length will have an impact on the

calculation, the 1/5 runner length cell model described above and the full-sized cell model of 300 mm were simulated by Fluent. The standard for determining the convergence was set as $<1 \times 10^{-7}$ to ensure the calculation accuracy of the resistance coefficient, and there was no or minimal pressure fluctuation in the pressure inlet and outlet sections (Han et al. 2016). According to eq. 2, MATLAB was used to fit the calculated pressure drop and velocity data, as shown in Fig. 5. The fitting results are shown in eqs. 4 and 5, where v is the velocity. The goodness of fit of the two curves was 1. The fitted velocity pressure drop curve must cross the origin, that is the closer the conic constant term is to the origin,

422

Trans. Can. Soc. Mech. Eng. Vol. 44, 2020

Fig. 4. Mesh generation of the hot side 1/5 fin element in main flow. [Colour online.]
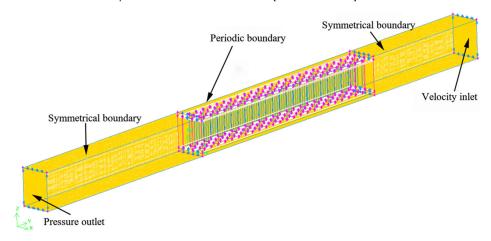

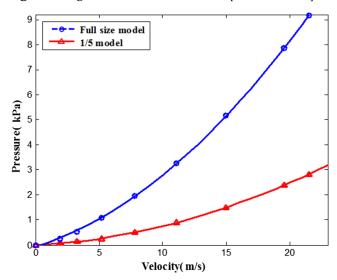**Fig. 5.** Fitting results of the fin element. [Colour online.]

Table 1. Resistance coefficients of different flow passage length.

	Inertial resistance	Viscosity resistance
Full-sized model	21.5	22 753 576
1/5-sized model	21	22 750 657

the higher the simulation accuracy (Zhang et al. 2016). According to eq. 2, the viscous resistance coefficient and inertial resistance coefficient were calculated as shown in Table 1. It can be seen that the resistance coefficient of the 1/5 flow channel length element was basically the same as that of the full-sized element when the mesh mass reached 1×10^{-10}. In this paper, through multiple simulation calculations, it was found that the difference between the resistance coefficient and the full-sized model gradually increased when the flow

passage length of the hot-side element decreased to 50 mm. It is considered that the simulation difference between the full-sized model, A, and the simulation difference, Δ, scaling model is affected by the scaling factor, C, and the grid quality, B (as shown in eq. 6). The simulation value of the scaling model is the function of the mesh quality, B, and scaling factor, C, which can theoretically shorten the flow path length of the cell body indefinitely when the mesh quality is infinitely high. However, because the mesh quality is difficult to control due to the complexity of the model, the size of the model needs to be adjusted according to the actual mesh quality to improve the solving efficiency.

The full-sized model:

$$(4) \qquad \Delta P = 8.36v^2 + 155.9v + 6.73$$

The 1/5-sized model:

$$(5) \qquad \Delta P = 1.713v^2 + 3.12v + 1.566$$

$$(6) \qquad |A - \delta(B,C)| = \Delta$$

3.2. Influence of boundary conditions on drag coefficient

The influence of periodic boundary and symmetric boundary on the calculation was studied by taking the hot side D1 element as an example. When the boundary conditions were set in Fluent, the periodic boundary and symmetric boundary were set respectively on the side of the element body, as shown in Fig. 6. However, the premise of using periodic boundary is that the shape, number of nodes, and mesh generation of the two surfaces must be completely consistent, which is greatly restricted by the model structure, while the symmetric boundary does not need to be considered. The resistance coefficient and inertial resistance coefficient of the symmetric boundary model are as shown in Table 2.

The symmetry boundary:

$$(7) \qquad \Delta P = 1.695v^2 + 3.21v + 1.51$$
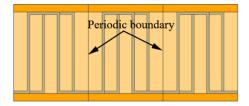
Fig. 6. Section of the fin element. [Colour online.]

Table 2. Resistance coefficients of the symmetric boundary.

Symmetrical boundary inertial resistance	Symmetric boundary viscous resistance
21.27	23 423 815

The periodic boundary of the finned part in the 1/5 element body model in Fig. 3 was changed to a symmetric boundary for simulation, and the calculation results were fitted as shown in eq. 7. There was no significant difference between the viscosity resistance coefficient and inertia resistance coefficient (Tables 1 and 2). This is because the rectangular staggered fin is a regular structure, and its porosity will not change regardless of the use of a periodic or symmetric boundary. Although the model cross section with symmetric boundary is consistent with the model with periodic boundary, the distribution of pressure field between them is almost approximate.

3.3. Boundary layer analysis of element model

The turbulence model of high Reynolds number is a standard model for fully developed turbulence (Mezher et al. 2013). It is suitable for solving flows in the turbulent core region, while the solution of the near wall part needs the help of the wall function. The boundary layer density required by different wall functions is also different. In theory, the boundary layer can be replaced by continuous densification of the grid near the wall surface, but this will increase the number of grids in the whole model and reduce the solution economy, so the boundary layer thickness needs to be calculated (Liu et al. 2015). In this paper, the maximum Reynolds number on the cold side and hot side is 2200 and 5000, respectively, which means the boundary layer effect on the hot side needs to be considered. In this paper, the cell model used the enhanced wall function to calculate the boundary layer thickness, when the y^+ is 1. The thickness of the starting layer was 0.01 mm, and there were five boundary layers in total.

$$(8) \quad y^+ = \frac{\rho \mu_\tau y_P}{\mu}$$

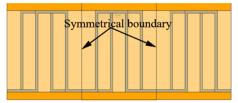$$(9) \quad \mu_\tau = \sqrt{\frac{\tau_\omega}{\rho_\omega}}$$

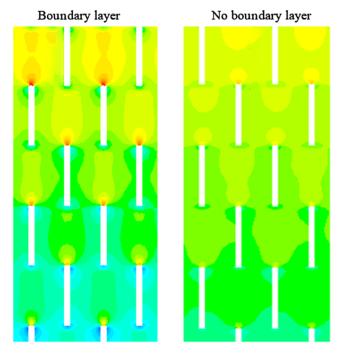**Fig. 7.** Influence of boundary layer on the pressure field. [Colour online.]

Table 3. Resistance coefficients without the boundary layer.

Borderless inertial resistance	Borderless viscous resistance
71	22 750 657

The comparison of static pressure cloud diagram at the center section of the unit body is shown in Fig. 7. It can be seen that the static pressure cloud diagram of the unit model with boundary layer is clearly arranged on the side of the near wall. However, the static pressure cloud diagram without boundary layer is quite different from the real flow field inside the intercooler. That is because the near wall part and the main flow field are solved according to the non-viscous flow. After calculation, the model resistance coefficient of the element without boundary layer is shown in Table 3, which is significantly different from the data in Table 1.

Table 4. Resistance coefficients of the hot and cold sides.

	D1		D2	
	Inertial resistance	Viscous resistance	Inertial resistance	Viscous resistance
Hot side	21	22 750 657	154.2	29 790 384
Cold side	47	9 618 697	880	29 662 220

Table 5. Lateral resistance coefficient combination in D2.

	Hot side		Cold side	
	Inertial resistance	Viscous resistance	Inertial resistance	Viscous resistance
1	154.2	29 790 384	880	29 662 220
2	2100	2 275 065 700	4700	961 869 700
3	21 000	22 750 657 000	47 000	9 618 697 000

Since the total thickness of the five-layer boundary layer, which is half of the mesh size of the main channel area, is ~0.05 mm, omitting the boundary layer is equivalent to completely ignoring the wall friction. However, the fin in the flow field is a typical longitudinal flow around the plate, and the incoming flow on the surface of the fin will be subject to non-negligible friction resistance. If the influence is ignored, the calculation result of the resistance coefficient will be greatly deviated.

3.4. Comparison of drag coefficients in different directions

The heat side and cold side D2 direction element models were established and their respective viscous resistance coefficients and inertial resistance coefficients were simulated according to the above methods, as shown in Table 4. The fitting results are shown in eqs. 10–12. According to the results obtained by the element solution method, the inertial resistance coefficient in the D2 direction of the hot side was 7.3 times of that in the D1 direction, and the viscous resistance coefficient was 1.3 times of that in the main flow direction. The inertial resistance in the D2 direction on the cold side was 18.7 times of that in the D1 direction, and the viscous resistance was 3.1 times of that in the main flow direction.

The hot side D2:

$$(10) \quad \Delta P = 19.86v^2 + 6.6v + 1.5716$$

The cold side D1:

$$(11) \quad \Delta P = 2868.8v^2 + 824.13v + 1.9082$$

The cold side D2:

$$(12) \quad \Delta P = 30086v^2 + 1429.6v + 2.1855$$

Fig. 8. Experimental acquisition process. [Colour online.]

4. Experiment contrast analysis

To verify the influence of transverse flow on the simulation calculation of the intercooler, the three resistance coefficient combinations in Table 5 were used for the overall simulation analysis. In the D2 direction of the first set of data, the viscous resistance coefficient and inertial resistance coefficient obtained by the unit body fitting as shown above were taken. The second set of data had a 100 times larger direct amplification in the D1 direction. The third set of data had a 1000 times larger direct amplification in the D1 direction. The data in Table 4 were used to find the resistance coefficient of the hot side D1 direction and the cold side D1 direction, without considering the influence of fluid flow in the D3 direction. The experiment was constructed as shown in Fig. 8. The experimental results of the water-cooled intercooler were compared with the overall simulation

Fig. 9. The contours of static pressure. [Colour online.]

Fig. 10. Pressure loss comparison on the cold side. [Colour online.]
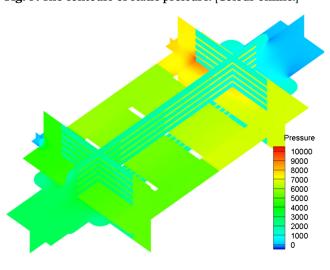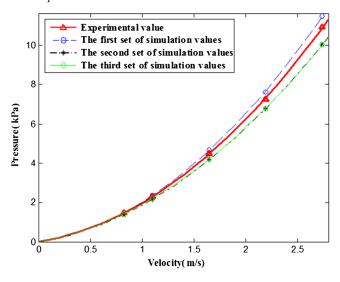

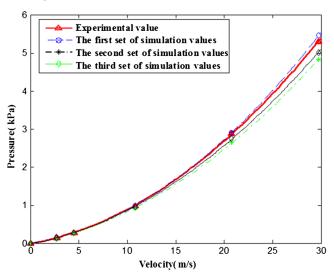**Fig. 11.** Pressure loss comparison on the hot side. [Colour online.]

results of the intercooler with several combinations of different drag coefficients.

The viscous resistance coefficient and inertial resistance coefficient were input into the porous zone model to simulate the whole model of the intercooler at different inlet speeds, and the porosity of the hot side and cold side of the water-cooled intercooler were 0.889 and 0.859, respectively. The static pressure cloud diagram of the intercooler when the coolant inlet velocity is 1.09 m/s and the pressurized air velocity is 4.5 m/s is shown in Fig. 9.

The results of the bench test of the water-cooled intercooler were compared with the overall simulation results of several intercooler combinations with different drag coefficients (Table 5). The comparison of cooling fluid lateral pressure is shown in Fig. 10. The D2 lateral

resistance coefficient curve obtained by using transverse element body was the closest to the test curve. The fitting curves of the second and third sets of data using the empirical method had a large deviation from the test value in the velocity interval. The critical value of the resistance coefficient was within 100 times of the main flow direction. After reaching the critical value, the lateral flow was basically in a suppressed state, so the curves of the second and third data sets in Fig. 10 are substantially coincident. The average deviation between the simulation value and the test value of the three combinations was 7.88%, 13.15%, and 13.95%.

Compared with the cold side, the hot side was greatly affected by transverse flow. The average deviations of the three sets of simulation values with that of the test values were 8.17%, 12.81% and 14.27%. From Figs. 10 and 11, lateral flow on the cold side was not obvious, while a considerable part of the flow on the hot side turns into lateral flow, which had a great influence. As the pressure drop of the heat exchanger is mainly the pressure loss along the way, it is considered that it is mainly affected by the following three points: (*i*) The inlet velocity of the fluid medium. The maximum velocity of the hot side pressurized air was 10.8 times that of the coolant. (*ii*) Ethylene glycol dynamic viscosity is far higher than that of pressurized air. (*iii*) The characteristic length of the fin itself is different. This leads to the fact that when the fluid medium is a gas, it is easy to flow to the lateral shunting, while liquid medium is not easy to shunt. That is, only a small lateral resistance coefficient is required for the simulation of the liquid medium, while a large lateral resistance coefficient is required for the simulation of the gas medium. It can be seen that the empirical method directly expands by two or three orders of magnitude according to the first direction to estimate the transverse resistance coefficient, which is more suitable

for simulating the liquid–liquid heat exchanger. Although the method of solving the element body to obtain the lateral resistance coefficient improves the accuracy of the simulation, it should not be ignored that it requires a lot of extra work to solve the lateral resistance coefficient alone. However, by defining the lateral resistance coefficient in an empirical way, the work efficiency can be improved. According to specific engineering problems, it is necessary to decide whether to pursue high-precision quantitative analysis or simple qualitative analysis.

5. Conclusion

In this research, the viscous and inertial resistance coefficients of the heat exchanger were solved using the finned element method. The results show that the transverse flow had a certain influence on the simulation calculation of the heat exchanger, which is closely related to the physical parameters of the fluid medium and the geometric measurements of the fin. Both the empirical method and the element method can accurately describe the flow field inside the heat exchanger, but the latter had a higher accuracy and the simulation results were closer to the experimental values. The empirical method was more suitable for simple analysis with a low accuracy requirement, while the element solution method was suitable for quantitative analysis with a certain accuracy requirement.

References

Balaji, N., Kumar, P.S.M., Velraj, R., and Kulasekharan, N. 2015. Experimental investigations on the improvement of an air conditioning system with a nanofluid-based intercooler. Arabian J. Sci. Eng. **40**(6): 1681–1693. doi:10.1007/s13369-015-1644-7.

Chen, Y.-P., Sheng, Y.-J., Dong, C., and Wu, J.-F. 2013. Numerical simulation on flow field in circumferential overlap trisection helical baffle heat exchanger. Appl. Therm. Eng. **50**(1): 1035–1043. doi:10.1016/j.applthermaleng.2012.07.031.

Cuevas, C., Makaire, D., and Ngendakumana, P. 2011. Thermohydraulic characterization of an automotive intercooler for a low pressure EGR application. Appl. Therm. Eng. **31**(14–15): 2474–2484. doi:10.1016/j.applthermaleng.2011.04.013.

Dong, J., Chen, J., Chen, Z., and Zhou, Y. 2007a. Air-side thermal hydraulic performance of offset strip fin aluminum heat exchangers. Appl. Therm. Eng. **27**(2–3): 306–313. doi:10.1016/j.applthermaleng.2006.08.005.

Dong, J., Chen, J., Chen, Z., Zhou, Y., and Zhang, W. 2007b. Heat transfer and pressure drop correlations for the wavy fin and flat tube heat exchangers. Appl. Therm. Eng. **27**(11–12): 2066–2073. doi:10.1016/j.applthermaleng.2006.11.012.

Dong, J., Su, L., Chen, Q., and Xu, W. 2013. Experimental study on thermal-hydraulic performance of a wavy fin-and-flat tube aluminum heat exchanger. Appl. Therm. Eng. **51**(1–2): 32–39. doi:10.1016/j.applthermaleng.2012.09.018.

Dong, W., Mao, C., Zhu, J.-J., and Chen, Y. 2012. Numerical and experimental analysis of inlet non-uniformity influence on intercooler performance. Proc. ASME Turbo Expo 2012: Turbine Technical Conference and Exposition. Volume 5: Manufacturing Materials and Metallurgy; Marine; Microturbines and Small Turbomachinery; Supercritical

CO$_2$ Power Cycles, Copenhagen, Denmark, 11–15 June 2012. pp. 349–357. doi:10.1115/GT2012-69231.

Guo, L., Qin, F., Chen, J., and Chen, Z. 2008. Lubricant side thermal-hydraulic characteristics of steel offset strip fins with different flow angles. Appl. Therm. Eng. **28**(8–9): 907–914. doi:10.1016/j.applthermaleng.2007.07.005.

Han, H., Li, B., and Shao, W. 2016. Effect of flow direction for flow and heat transfer characteristics in outward convex asymmetrical corrugated tubes. Int. J. Heat Mass Transfer, **92**: 1236–1251. doi:10.1016/j.ijheatmasstransfer.2014.11.076.

Hribernik, A., and Moskwa, J.J. 2000. Transient response of a cross-flow charge air intercooler and its influence on engine operation. J. Dyn. Syst., Meas., Control, **122**(3): 483–489. doi:10.1115/1.1286683.

Kays, W.M., and London, A.L. 1984. Compact heat exchangers. McGraw-Hill, New York, NY, USA.

Kumar, N.S., Dhinakarraj, C.K., Deepanraj, B., Babu, N.M., and Santhoshkumar, A. 2012. Modification and analysis of compressor intercooler fin in turbocharger using FEM. Procedia Eng. **38**(2): 379–384. doi:10.1016/j.proeng.2012.06.047.

Li, Z., Zhang, H.-B., Wen, X.-Y., and Xiao, D.-M. 2008. Numerical simulation of an intercooler for a complex-cycle marine gas turbine. J. Eng. Therm. Energy Power, **23**(2): 148–152.

Liu, J.J., Liu, Z.C., and Liu, W. 2015. 3D numerical study on shell side heat transfer and flow characteristics of rod-baffle heat exchangers with spirally corrugated tubes. Int. J. Therm. Sci. **89**: 34–42. doi:10.1016/j.ijthermalsci.2014.10.011.

Mezher, H., Migaud, J., Raimbault, V., Lelong, J.-G., Chalet, D., Perrot, N., et al. 2013. Optimized air intake for a turbocharged engine taking into account water-cooled charge air cooler reflective properties for acoustic tuning. SAE Technical Paper 2013-01-0575. doi:10.4271/2013-01-0575.

Song, X., Myers, J., and Sarnia, S. 2014. Integrated low temperature cooling system development in turbo charged vehicle application. SAE Int. J. Passeng. Cars — Mech. Syst. **7**(1): 163–173. doi:10.4271/2014-01-0638.

Uysal, A., Ozalp, A.A., Korgavus, A., and Korgavus, O. 2012. Numerical modeling of the momentum and thermal characteristics of air flow in the intercooler connection hose. Int. J. Adv. Manuf. Technol. **60**(5–8): 811–824. doi:10.1007/s00170-011-3591-0.

Xu, Z. 2016. Research on heat dissipation characteristics of water-air intercooler for construction vehicle. School of Mechanical and Aerospace Engineering, Jilin University, Changchun, China.

Yu, C., Qin, S., Liu, Y., and Chai, B. 2018. Heat exchange performance optimization of a wheel loader cooling system based on computational fluid dynamic simulation. Adv. Mech. Eng. **10**(11). doi:10.1177/1687814018803984.

Zhang, Q., Qin, S., and Ma, R. 2016. Simulation and experimental investigation of the wavy fin-and-tube intercooler. Case Stud. Therm. Eng. **8**: 32–40. doi:10.1016/j.csite.2016.04.003.

List of symbols

D_{ij}	viscous resistance coefficient
C_{ij}	inertial resistance coefficient
G_k	kinetic energy caused by the average velocity gradient
G_b	turbulent energy generated by the buoyancy effect
S_i	source term
v	flow velocity vector
μ	viscosity
ρ	density